Analyst

ROYAL SOCIETY OF CHEMISTRY

PAPER

View Article Online
View Journal | View Issue

Cite this: *Analyst*, 2025, **150**, 3880

Mass spectrometry imaging of lipids in a gut epithelial cell model†

Qianying Xu, [a] Hadeer Mattar, [b] Emmanuelle Claude,[c] Lee Gethings [a,c,d] and E. N. Clare Mills *[a,d]

Scope: The Caco2/HT29-MTX co-culture system is widely used as a cell model of the intestinal epithelium. Although the gut epithelium plays an important role in the uptake of free fatty acids and the resynthesis of triglycerides, the lipid distribution profile of the two-dimensional co-culture system is not well understood. Desorption electrospray ionisation (DESI) mass spectrometry (MS) imaging has been widely used to study the main classes of lipid molecules on different tissues. This has been used to map the lipid distribution in the Caco2–HT29-MTX co-culture system. *Methods and results*: Caco2 and HT29-MTX cells were seeded on coverslips either individually or as co-cultures at different ratios. Cells were cultured for 21 days before MS imaging using a DESI source in both positive and negative ionisation modes, with the identity of the selected lipid confirmed using tandem MS. Although many lipids were common to both cell lines, there were distinctive patterns in the lipidomes. Thus, the lipidome of Caco2 cells was more heterogeneous and richer in cholesterol esters and certain triglycerides while HT29-MTX cells have a distinctive lipidome including phosphatidylethanolamines and odd chain phosphatidylcholines and C17 fatty acids. *Conclusion*: DESI-MS imaging has shown that Caco2 and HT29-MTX cells have distinctive lipidomes that are still evident when the cells are co-cultured. It has the potential to both allow further validation of these widely used cell models and provide insights into how dietary components may modify lipid metabolism in the future.

Received 25th March 2025,
Accepted 24th June 2025

DOI: 10.1039/d5an00341e

rsc.li/analyst

Introduction

Cell-based models of the intestinal epithelium are often used to study intestinal transport of dietary molecules – from micronutrients, such as iron, to toxicants and allergens.[1–3] The mainstay of these models is the Caco2 cell line, which was derived from a human colorectal adenocarcinoma in 1977 and has since become the most widely used and best characterised intestinal cell line. It has the ability to mimic the morphological and functional characteristics of gut enterocytes by forming tight junctions between the cells and differentiating to form a brush border with microvilli on the apical surface of the cell.[1] An important metabolic activity of the enterocytes *in vivo* is the uptake of free fatty acids from the apical side and their re-synthesis into triglycerides, which are then secreted on the basolateral side prior to being transported in the lymphatic system. Consequently, the enterocytes control the passage of lipids from food into the body and there is increasing evidence that this may be modulated by dietary components, such as polyunsaturated fatty acids, as well as products of microbial metabolism, such as short chain fatty acids.[4] Although Caco2 cells have been widely used to study lipid uptake and transport over many years,[5–10] they have several limitations as, even when differentiated, they retain much of the character of cancer cell lines.[11] Furthermore, they cannot mimic the combination of differentiated cell types found in the intestinal epithelium, such as goblet cells (mucus producing cells), endocrine cells, and M cells, and consequently lack a mucus layer. These limitations can be addressed by using co-culture systems, one of which employs HT29-MTX cells that can act as model goblet cells[12] and has been optimised with respect to the seeding ratios of Caco2 and HT29-MTX cells.[13] In addition to providing a mucus layer, co-culturing Caco2 and HT29-MTX cells has also been shown to rescue the epithelial phenotype of the Caco2 cells, an effect that is further enhanced through interactions mediated by dietary compounds such as oleic acid.[11]

Although well characterised using classical cell biological methods and gene expression analysis,[14,15] metabolomic and

[a]*Division of Immunology, Immunity to Infection and Respiratory Medicine, School of Biological Science, Wythenshawe Hospital, University of Manchester, UK. E-mail: clare.mills@surrey.ac.uk, clare.mills@manchester.ac.uk*
[b]*Faculty of Applied Medical Science, Al Baha University, Saudi Arabia*
[c]*Waters Corporation, Wilmslow, UK*
[d]*School of Biosciences, University of Surrey, Guildford, UK*

† Electronic supplementary information (ESI) available. See DOI: https://doi.org/10.1039/d5an00341e

lipidomic characterisation has been more limited, focusing on, for example, sphingolipids involved in regulating tumour growth.[16–18] However, the visualisation of lipid distribution on the 2D co-culture system is still lacking. A highly effective technique for mapping metabolites, such as lipids, in biological samples is mass spectrometry (MS) imaging; the abundance and high ionisation efficiency of lipids enables the detection of many different lipid species based on their mass to charge ratios. It can be performed without the need for deuterated lipid standards[19] and can enable detailed mapping across length scales from subcellular resolution, as can be achieved with methods such as secondary ionisation MS (SIMS), to meso-scale resolution of 50–100 μm enabled by desorption electrospray ionisation (DESI) MS imaging.[20] Consequently, MS imaging has been used to provide insights into the spatial distribution of lipids in various types of cells and tissues, supporting, for example, improved diagnosis of diseases such as cancer[19,21] and has previously been applied to study different lipid species and their special arrangement in cell cultures.[19,22] DESI MS imaging overcomes many of the limitations of other MS imaging methods. For instance, its ability to ionise lipids under ambient conditions means minimal sample preparation is required and it does not require a matrix to extract the analytes from a sample surface,[23] nor does it require tissues or cells to be mounted onto specific substrates as is required for SIMS.[20] In addition, the ionisation of the analyte using DESI takes place outside the vacuum system to avoid a possible delay in the analysis time and to prevent contamination of target analytes[24] and provides the resolution required to highlight any heterogeneity in 2D cell cultures. Therefore, an exploratory study has been undertaken to apply MS imaging to mapping the lipids in Caco2 and HT29-MTX cells, grown alone and together in confluent 2D cell cultures. This has demonstrated variation across the confluent 2D cultures, likely reflecting metabolic differences identified in individual and small clusters of cells.

Materials and methods

Reagents

Two different batches of Caco2 (HTB-37™) and HT29-MTX cell lines were purchased from the European Type Culture Collection ATCC (Teddington London, UK) in 2018 (batch 1) and again in 2022 (batch 2). Dulbecco's modified Eagle's medium (DMEM) without L-glutamine, Dulbecco's phosphate-buffered saline (DPBS), foetal bovine serum albumin (FBS), trypan blue solution (0.4% (w/v)) and analytical grade ammonium acetate were purchased from Sigma-Aldrich (Dorset, UK). Sodium pyruvate, amphotericin B, and a live/dead staining kit were purchased from Thermo Fisher Scientific (Hertfordshire, UK) while penicillin/streptomycin and L-glutamine were from Invitrogen (Shropshire, UK). A C-Chip disposable haemocytometer was purchased from Labtech International Ltd (Heathfield, UK). Borosilicate glass coverslips with thicknesses of 1.5 and 18 mm or 25 mm ∅ were purchased from VWR (Leicestershire, UK). Cell culture plasticware was purchased from either Cellstar or Greiner Bio-One (Stonehouse, UK). All other reagents (at least of analytical reagent grade) and plasticware were purchased from Sigma-Aldrich (Dorset, UK).

Sample preparation

Caco2 and HT29-MTX cells were cultured separately in bulk in 25 cm^2 flasks at 37 °C with 5% CO_2 for 2–3 days. DMEM complete medium supplemented with 20% (v/v) foetal bovine serum, 2% (w/v) L-glutamine, 1% sodium pyruvate, 1% (w/v) penicillin–streptomycin and 0.01% amphotericin B was used as complete culture medium. Passage P9 was used for Caco2 and P19 for HT29-MTX after thawing. On reaching 80–90% confluency, cells were trypsinised and then seeded onto multiple coverslips to generate replicates at a density of 1×10^5 cells per mL. These cells were either cultured separately or in a co-culture system, with ratios of 90 : 10, 75 : 25, 50 : 50 and 25 : 75 (Caco2 : HT29-MTX cells). For each condition, four biological replicates were prepared. After seeding, each coverslip was placed in a well of 6-well cell culture plates and incubated at 37 °C with 5% CO_2. The medium was changed every 48 hours for 21 days until cells were confluent. Coverslips were prepared for DESI MS imaging analysis by rinsing with 150 mM ammonium acetate (pH 7) for 30 seconds before being allowed to dry in the air stream of a biological safety cabinet for 15 minutes. The coverslips were then thoroughly dried using a vacuum desiccator for another 15 minutes before storage at −80 °C until analysed.

Cell viability staining

Staining was performed according to the kit instructions. Briefly, the staining solution was prepared by adding 15 μL of ethidium homodimer (EthD-1) and 5 μL of calcein to 10 ml of DPBS. Cells were rinsed with pre-warmed DPBS (3 × 5 min) to remove any residual medium before adding 300 μl of the staining solution and incubating for 30–40 minutes at ambient temperature. The cells were imaged using a fluorescence microscope, EVOS FL (Life Technologies Ltd, Paisley, UK), using either a standard fluorescein bandpass filter (emission at 494 nm, green) for calcein or filters for propidium iodide (emission at 535 nm, red) for EthD-1. The green (live cells) and red (dead cells) images were then merged using a fluorescence microscope.

DESI MS imaging

Dried cell cultures grown on coverslips were mounted on microscope glass slides using double sided tape. The slides were imaged using light microscopy and images were scanned using an Epson Perfection V600 photo scanner. The scanned images were imported and the area where cells were confluent was selected using the co-registered photographic image of the samples in High-Definition Imaging (HDI) version 1.5 and version 1.7. Imaging experiments were carried out on a DESI (Prosolia, USA) mounted on a Xevo-G2-XS quadrupole-time of flight (QTOF) mass spectrometer (Waters Corporation,

Wilmslow, UK) with a mass measurement accuracy of 1 ppm. The DESI spray was composed of a solvent mixture of 98 : 2% MeOH : water (v/v) delivered at a flow rate of 2 μL min^{-1} with a nebulizing gas pressure of 5 bar. The sprayer's geometric positions were set such that the sprayer was 1.5 mm above the sample surface and the distance between the sprayer and the capillary was 6 mm. The source temperature was 150 °C. For both positive and negative ionization modes, the acquisition mass range was 50–1200 *m*/*z*. DESI MS imaging experiments were performed at a scan rate of 2 scans per second in positive mode and 4 scans per second in negative mode. The *X* and *Y* pixel sizes were set at 50 μm.

Selected precursor ions in both positive and negative ionisation modes were further analysed using MS/MS. The experiments were carried out on a DESI-XS (Prosolia, place, USA) mounted on a Xevo-G2-XS Q-TOF mass spectrometer (Waters Corporation, Wilmslow, UK). Spray conditions were the same as in DESI imaging. The spectra were visualised using MassLynx version 4.2 (Waters Corporation, Wilmslow, UK).

Data analysis

Raw data from each biological condition were processed using High Definition Imaging (HDI) software versions 1.5 and 1.7 (Waters Corporation, Wilmslow, UK) to obtain ion images from a consolidated list of *m*/*z* common to the different datasets as well as the unique *m*/*z*. The ion images were normalised to total ion current (TIC). Regions of interest (ROIs) were drawn directly from the DESI images that produced a .csv file containing average TIC normalised intensities, which was used for statistical analysis using MetaboAnalyst1 and 6.0 (**https://www.metaboanalyst.ca**)[25] to compare selected lipids that are present in the two cell lines. Similarly, MS imaging analysis of Caco2/HT29-MTX co-culture was performed using the same criteria as DESI images with the same precursor ions mentioned above. For pixel classification of DESI imaging datasets, Waters Corporation (WRC, Budapest, Hungary) prototype PCA-AMX MS imaging software was used in combination with HDI software (Fig. S11†), an approach previously used in a variety of applications such as meat speciation and classification of cells in tissues.[26–28]

Results

Development of cell cultures for MS imaging

Initially, pilot studies were conducted with the Caco-2 and HT29-MTX cell lines cultured alone and in co-culture on replicated glass coverslips, a substrate that is compatible with MS imaging requirements. The same culture conditions and seeding densities were applied when culturing the cells in the transwell system used to model the gut epithelium and study nutrient transport.

Initial pilot MS imaging studies were performed prior to the cells becoming confluent (Fig. S2†). This showed the capacity of the method to image individual cells and small clusters of HT29-MTX cells that are around 20 μm in diameter and illustrated the metabolic heterogeneity of the cell cultures especially with larger clusters.

Thus, when selecting three lipids, phosphatidylcholine (PC) 16:0_18:0 (*m*/*z* 798.55), PC 16:0_16:1 (*m*/*z* 770.52) and PC 38:4 (*m*/*z* 848.56) to provide images, one small region (Fig. S1A† inset) representing a group of two or three cells was mapped with a single lipid, *m*/*z* 770.51 (circled in green), while a small cluster of ~20–30 cells was represented by two lipid species (*m*/*z* 798.55 and 848.56; circles in purple). A very large cluster of cells was found to contain three of the PC species, including PC 38:4.

These data demonstrated the feasibility of imaging cells grown on coverslips by MS imaging. However, the aim of the study was to investigate the metabolic heterogeneity of cells grown as models of the gut epithelium. Thus, the remaining experiments were focused on cells grown to confluence. Cultures including the HT29-MTX cell line showed clear evidence of the production of mucus with an amorphous fluorescence green staining mass evident (Fig. S2b–d†). A small number of red-staining dead cells were observed scattered across the coverslips interspersing the live cells, especially in the cultures containing the HT29-MTX cells but the presence of the mucus obscured the images.

Lipid mapping of Caco2 and HT29-MTX

Subsequently, the lipid composition of replicate cultures of Caco2 and HT29-MTX cells (singly and in coculture) was characterised using DESI MS imaging in both positive and negative ionisation modes. Mass events relating to putative lipid species were selected and identified using a combination of accurate mass searching of the LipidMaps database and MS/MS analysis. Examples of combined spectra for the selected region of interest (ROI) from Caco2 and HT29-MTX cells are as shown in Fig. 1 and 2 respectively and the lipids identified in positive and negative ionisation modes are listed in Table 1.

Na^+, K^+, and NH_4^+ adducts were frequently identified in the spectra, a common occurrence as lipids have an affinity for sodium and potassium ions and ammonium was introduced in sample pre-treatment.

Major mass spectral features were reproducibly identified in both positive and negative ionisation modes for both cell types across a minimum of four replicate cultures and are discussed in detail below for one exemplar culture. The positive ionisation mode combined spectrum of the imaged Caco2 cells (Fig. 1a) was dominated by species ionising with a mass to charge ratio (*m*/*z*) in the range of 600–1000 *m*/*z*, which could be annotated as lipids (Fig. 1b). The most intense peak at *m*/*z* 798.55 and a less intense species at *m*/*z* 770.51 corresponded to phosphatidylcholines with long chain fatty acids (16:0_16:1 and 16:0_18:1 respectively). Other peaks at *m*/*z* 633.49 and 659.51 were identified as cholesterol esters (CE 14:1 and 16:2 respectively), and a peak at *m*/*z* 897.75 corresponded to a triglyceride (TG 52:2) (Fig. 1b and Table 1). Fewer species were observed in negative ionisation mode (Fig. 1d) and included putative lipid species at *m*/*z* 281.25 and 309.28 corresponding

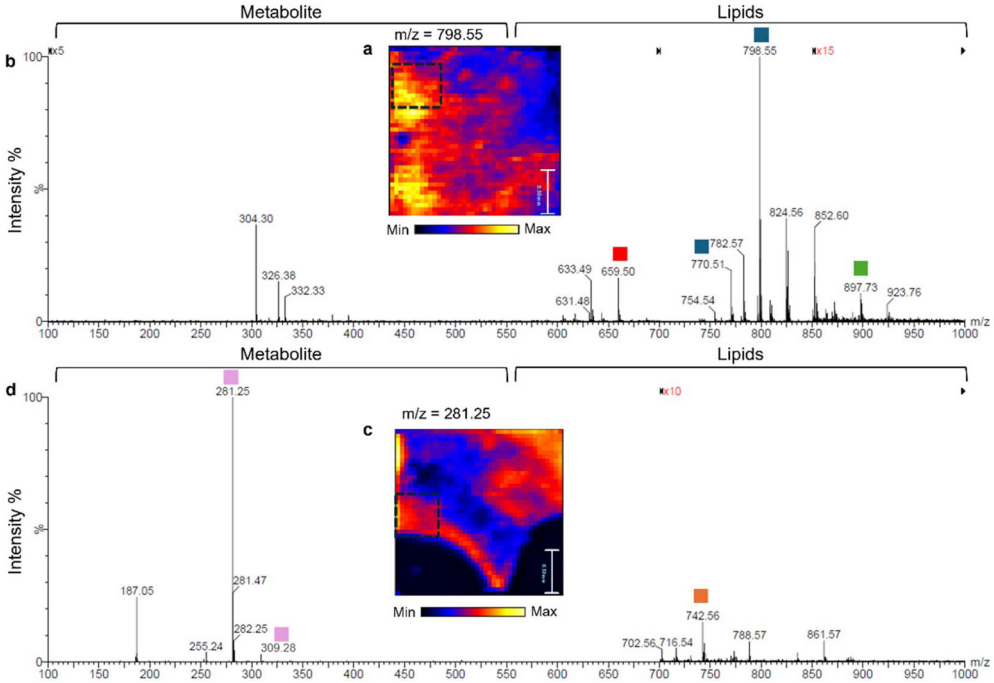

Fig. 1 Combined mass spectra of ROI from a MS image of Caco2 cells collected in positive (a and b) and negative (c and d) ionisation modes. MS images of cells collected in positive (a) and negative (c) ionisation modes coloured by intensity for lipid species. The black dotted box represents the ROI from which the combined mass spectra were derived for either positive (b) or negative (d) ionisation mode. The lipid ions selected for DESI MS imaging are indicated as follows: positive ionisation mode: red – cholesterol ester; dark-blue – phosphatidylcholine; and green – triglycerides. Negative ionisation mode: pink – fatty acids (oleic acid [*m*/*z* 281.25] and eicosenoic acid [*m*/*z* 309.28]) and orange – phosphatidylethanolamine.

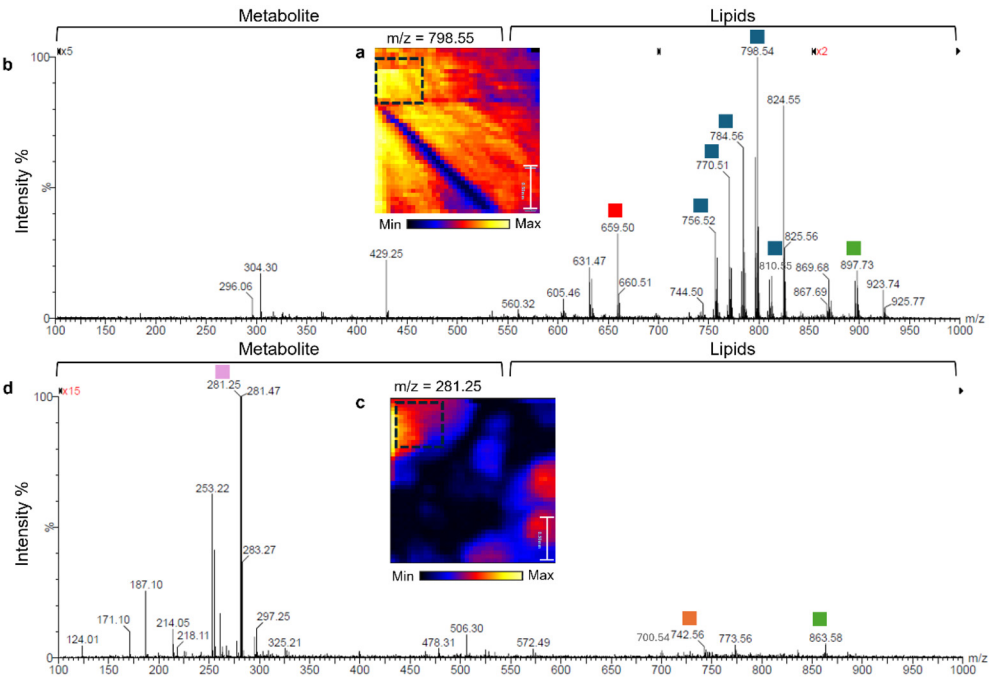

Fig. 2 Combined mass spectra of a ROI from a MS image of HT29-MTX cells collected in positive (a and b) and negative ionisation modes. MS images of cells collected in positive (a) and negative (c) ionisation modes coloured by intensity for lipid species. The black dotted box represents the ROI from which combined spectra were derived for either positive (b) or negative (d) ionisation mode. The lipid ions selected for DESI MS imaging are indicated as follows: positive ionisation mode: red – cholesterol ester; dark-blue – phosphatidylcholine; and green – triglycerides.

Table 1 Summary of lipid molecules identified in the average mass spectra for DESI images taken in positive and negative ionisation modes. Lipid species identified from averaged DESI mass spectra of Caco2, HT29-MTX cell cultures and co-cultures collected in positive and negative ionisation modes were identified either by accurate mass matching using the LipidMaps database (https://www.lipidmaps.org) or by MS-MS analysis

Lipid	Experimental *m/z*	Theoretical *m/z*	Mass Error	Formula	MS/MS	Cultures					
						Caco2	90 : 10 Caco2 : HT29-MTX	75 : 25 Caco2 : HT29-MTX	50 : 50 Caco2 : HT29-MTX	25 : 75 Caco2 : HT29-MTX	HT29-MTX
Positive ionisation mode											
CE (14:1) $[M + K]^+$	633.49	633.50	0.01	$C_{41}H_{70}O_2K$	N/A	Yes	Yes	Yes	Yes		
CE (16:2) $[M + K]^+$	659.51	659.51	0.00	$C_{43}H_{72}O_2K$	N/A	Yes	Yes	Yes	Yes	Yes	Yes
PC (31:1) $[M + K]^+$	756.53	756.55	0.02	$C_{39}H_{76}NO_8PK$	Yes		Yes	Yes	Yes	Yes	Yes
PC (16:0_ 16:1) $[M + K]^+$	770.51	770.50	0.01	$C_{40}H_{78}NO_8PK$	Yes	Yes	Yes	Yes	Yes	Yes	Yes
PC (32:0) $[M + K]^+$	772.54	772.53	0.01	$C_{40}H_{80}NO_8PK$	N/A				Yes	Yes	Yes
PC (O-34:1) $[M + K]^+$	784.55	784.56	0.01	$C_{42}H_{84}KNO_7P$	Yes				Yes	Yes	Yes
PC (16:0; 18:1) $[M + K]^+$	798.55	798.54	0.01	$C_{42}H_{82}NO_8PK$	Yes	Yes	Yes	Yes	Yes	Yes	Yes
PG (38:4) $[M + H]^+$	799.55	799.55	0.00	$C_{44}H_{79}O_{10}P$	N/A	Yes	Yes	Yes	Yes	Yes	
PC (34:0) $[M + K]^+$	800.57	800.56	0.01	$C_{42}H_{84}NO_8PK$	N/A	Yes	Yes	Yes	Yes	Yes	Yes
PC (17:1_ 18:1) $[M + K]^+$	810.55	810.52	0.03	$C_{43}H_{82}NO_8PK$	Yes	Yes	Yes	Yes	Yes	Yes	Yes
PC (36:2) $[M + K]^+$	824.55	824.54	0.01	$C_{44}H_{84}NO_8PK$	N/A	Yes	Yes	Yes	Yes	Yes	Yes
TG 49:8 $[M + Na]^+$	827.60	827.61	0.01	$C_{52}H_{84}O_6Na$	N/A	Yes	Yes	Yes	Yes	Yes	
TG (48:1) $[M + K]^+$	843.68	843.67	0.01	$C_{51}H_{96}O_6K$	N/A				Yes	Yes	Yes
TG (16:1_ 16:1_20:0) $[M + K]^+$	897.72	897.72	0.00	$C_{55}H_{102}O_6K$	N/A	Yes	Yes	Yes	Yes	Yes	Yes
TG (54:3) $[M + K]^+$	923.74	923.74	0.00	$C_{57}H_{104}O_6K$	N/A	Yes	Yes	Yes	Yes	Yes	Yes
Negative ionisation mode											
FA (12:6) $[M–H]^-$	187.04	187.07	0.03	$C_{12}H_{12}O_2$	N/A	Yes	Yes	Yes	Yes	Yes	Yes
FA (10:3) $[M + Cl]^-$	201.04	201.06	0.02	$C_{10}H_{14}O_2$	N/A	Yes	Yes	Yes			
FA (16:0) $[M–H]^-$	255.23	255.23	0.00	$C_{16}H_{32}O_2$	N/A	Yes	Yes	Yes	Yes	Yes	Yes
FA (18:1) $[M–H]^-$	281.25	281.24	0.01	$C_{18}H_{34}O_2$	N/A	Yes	Yes	Yes	Yes	Yes	Yes
FA (20:2) $[M–H]^-$	307.27	307.26	0.01	$C_{20}H_{36}O_2$	N/A	Yes	Yes	Yes	Yes	Yes	Yes
FA (20:1) $[M–H]^-$	309.28	309.27	0.01	$C_{20}H_{38}O_2$	N/A	Yes	Yes	Yes	Yes	Yes	
LPA (20:0) $[M–H]^-$	465.33	465.30	0.03	$C_{23}H_{47}O_7P$	N/A		Yes	Yes	Yes	Yes	Yes
LPE (22:4) $[M–H]^-$	528.28	528.30	0.02	$C_{27}H_{48}NO_7P$	N/A		Yes	Yes	Yes	Yes	Yes
PE (O-32:2) $[M–H]^-$	672.50	672.49	0.01	$C_{37}H_{72}NO_7P$	N/A		Yes	Yes	Yes	Yes	Yes
PE (O-34:2) $[M–H]^-$	700.53	700.52	0.01	$C_{39}H_{76}NO_7P$	Yes				Yes	Yes	Yes
PE (36:2) $[M–H]^-$	742.54	742.53	0.01	$C_{41}H_{78}NO_8P$	Yes	Yes	Yes	Yes	Yes	Yes	Yes
PG (36:2) $[M–H]^-$	773.55	773.55	0.00	C42H79O10P	Yes	Yes	Yes	Yes	Yes	Yes	Yes
PI (36:1) $[M–H]^-$	863.58	863.56	0.02	$C_{45}H_{85}O_{13}P$	N/A				Yes	Yes	Yes
PI (O-39:2) $[M–H]^-$	889.62	889.62	0.00	$C_{48}H_{91}O_{12}P$	N/A	Yes	Yes	Yes	Yes		

N/A – Not available. Dark grey shading indicates which cell culture type the putative lipid species was identified in. MS–MS spectra of identified lipids are provided in the ESI† as follows: *m/z* 770.51 – Fig. S3;† *m/z* 742.54 – Fig. S4;† *m/z* 773.53 – Fig. S5;† *m/z* 756.53 – Fig. S6;† *m/z* 784.56 – Fig. S7;† *m/z* 810.55 – Fig. S8.†

to oleic acid (18:1) and eicosenoic acid (20:1), respectively. MS/MS analysis allowed a peak of *m*/*z* 742.55 to be putatively identified as a phosphatidylethanolamine (Table 1) (Fig. S4†) while another peak at *m*/*z* 773.55 was identified as a phosphatidylglyceride (PG 18:1/18:1) with the loss of a hydrogen ion (Fig. S5†). Analysis of the MS/MS fragmentation showed a peak of *m*/*z* 491.28, which resulted from the loss of a ketene group. This then facilitated the specific loss of the fatty acid chain of 18:1. A fragment was also detected at *m*/*z* 417.25, which indicates the loss of the glycerol head group while another fragment detected at *m*/*z* 281.25 demonstrated the loss of the fatty acid chain of 18:1. HT29-MTX cells gave a similar combined positive ionisation mode mass spectrum to the Caco2 cells (Fig. 3c) with many of the same lipid species present. Three notable differences were observed. One of these was a lipid species with an *m*/*z* value of 756.55, which was only detected

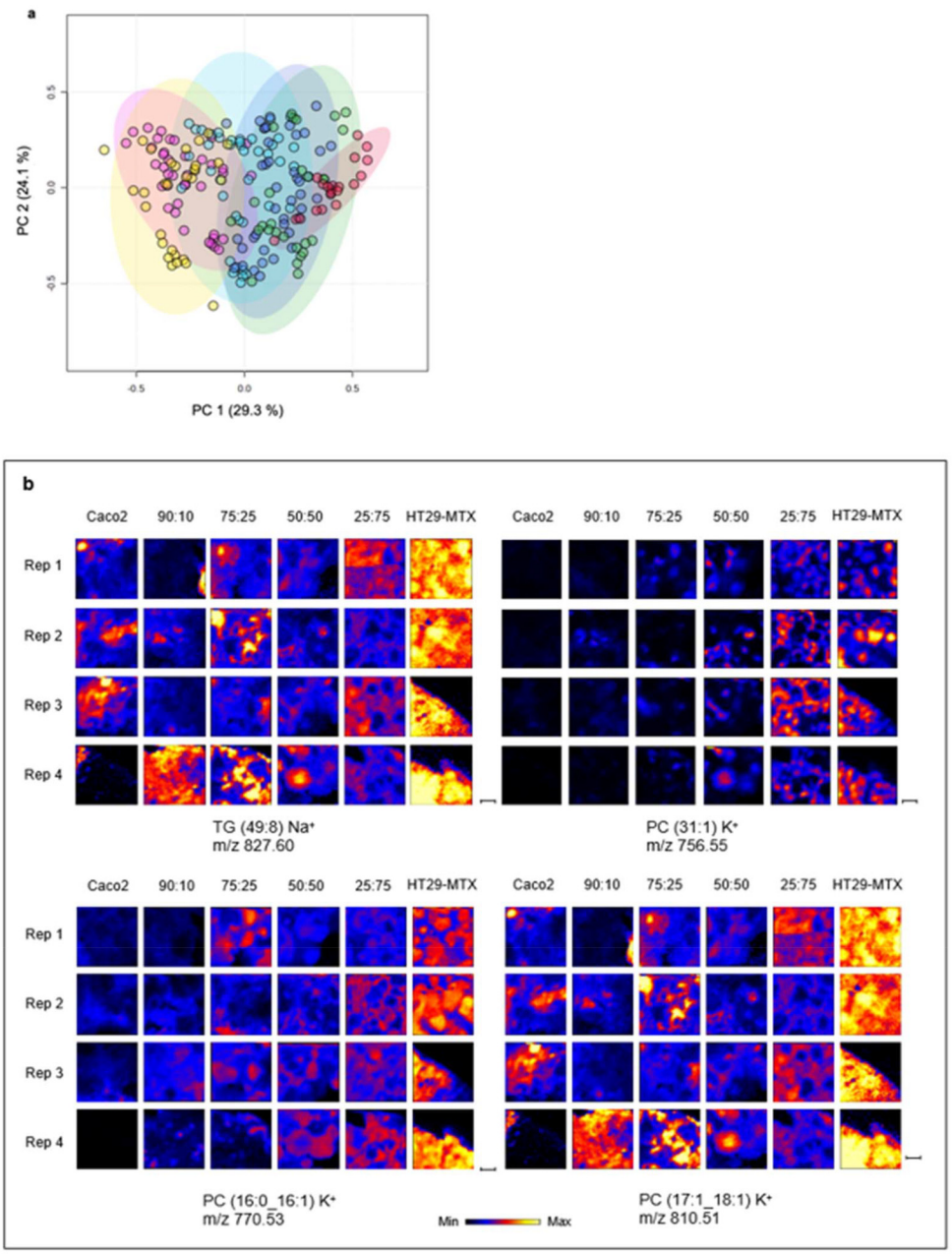

Fig. 3 Comparison of the spatial distribution of lipids in co-cultures of Caco2 and HT29-MTX cells imaged in positive ionisation mode. (a) PCA of ROIs, 0.05 mm^2 for each MS image, each dot representing one ROI coloured as follows: red – Caco2 cells; yellow – HT29-MTX; green – co-culture seeded with a ratio of Caco2–HT29-MTX cells of 90 : 10; purple – co-culture seeded with a ratio of Caco2–HT29-MTX cells of 75 : 25; blue – co-culture seeded with a ratio of Caco2–HT-29MTX cells of 50 : 50; pink – co-culture seeded with a ratio of Caco2–HT-29MTX cells of 25 : 75. Loadings (Fig. S9†) were used to identify lipids responsible for the clustering of ROIs; the distribution of these was then visualised across images (b). The scale bar = 0.05 mm. Lipid identifications are summarised in Table 1.

in the HT29-MTX cells and was identified as an unusual phosphatidyl choline with an odd chain fatty acid (PC 31:1). A second lipid with an *m*/*z* of 784.55 was identified as a phosphatidyl choline with an ether linked fatty acid (PC O-34:1), which was present in both cell types but more abundant in the HT29-MTX cells. A third lipid species observed only in the HT29-MTX cells had an *m*/*z* of 810.55, which was identified as PC (17:1_18:1) using MS/MS analysis (Fig. S8†). As the bonds attaching the phosphatidylcholine moiety to the glycerol backbone are the weakest, they break readily during the MS/MS fragmentation.

Consequently, phosphatidylcholines are characterised by neutral loss of the choline head group $N(CH_3)_3$ generating a fragment at *m*/*z* 751.47. The fragmentation also demonstrates the loss of fatty acid chains (17:1 and 18:1) at *m*/*z* 558.74 and 537.48. A similar mass shift was detected because of the loss of potassium (K+) associated with a fragment ion of *m*/*z* 589.53. Other lipid ions of *m*/*z* 672.51, 700.54, 722.53 and 863.60 were only observed in negative ionisation mode analysis of the HT29-MTX cells (Fig. 3c) and were putatively identified based on mass alone as phosphatidylethanolamine (PE) and phosphatidylinositol (PI) lipids, respectively.

Effect of co-culturing Caco2 and HT29-MTX cells on lipid composition

DESI imaging of the individual cell types was performed using co-cultures seeded with ratios of Caco2 : HT29-MTX cells of 90 : 10, 75 : 25, 50 : 50, and 25 : 75, spanning those used in uptake experiments.[29] Lipid features able to discriminate between the different cell types within the co-cultures were identified using PCA analysis of data collected from ROIs located in areas where the cells were identified by light microscopy to be confluent and were of sufficient size to allow the heterogeneity of the culture to be imaged.

Initially similarities and differences in lipid species between the Caco2 and HT29-MTX cell types were investigated in positive (ESI Fig. S11† and Fig. 3) and negative ionisation modes (ESI Fig. S12,† Fig. 4). They could be clearly separated based on principal component 1 (PC1), which accounted for a variation of 46.2%, while PC2 represented variance in different lipid classes identified (Fig. S11 and S12†). Imaging under both positive and negative ionisation modes showed variation between the ROIs from the replicate cultures, which was more marked for the Caco2 cells (Fig. S11a, S12a,† Fig. 3a and 4a). Lipid species contributing to the separation of Caco2 and HT29-MTX cells on PCA were selected and used to generate DESI MS images for particular lipid species identified in positive (ESI Fig. S11b, c† and Fig. 3b) and negative (ESI Fig. S12b, c† and Fig. 4b) ionisation modes. This showed heterogeneity within the replicate cultures but nevertheless demonstrated trends that were also observed in the PCA plot. Thus, the Caco2 cells tended to contain a higher level of cholesterol esters (CE 14:1) and phosphatidyl choline (PC 34:0), together with a phosphatidylglycerol (PG 38:4) and triglyceride (TG 49:8), with the latter having a higher intensity. In contrast, the HT29-MTX cells were enriched in several types of phosphatidyl choline, including PC 31:1 and PC 17:1_18:1 together with phosphatidyl choline of ether lipids, PC O-34:1 at *m*/*z* 784.57 (corresponding to lipids with either 16:0_18:1 or 18:0_16:1 fatty acid side chains) and PC 16:1_18:1 (ESI Fig. S11b and c†). It is clear from the images that these PCs were present in clusters of HT29-MTX cells and showed distinctive heterogeneity across the culture. The data acquired in positive ionisation mode showed that while PC 16:0_16:1 PC 31:1, and PC 17:1_18:1 were largely absent from Caco2 cells cultured alone, these lipids were identified at a low level in the low ratio (*e.g.* 90 : 10 Caco2–HT29-MTX) co-cultures, with the abundance increasing as the seeding ratio of HT29-MTX cells increased (Fig. 3b). In contrast, TG (49:8) tended to be more abundant in the singly cultured Caco2 cells and the 90 : 10, 75 : 25 and 50 : 50 co-cultures, but it was reduced in the 25 : 75 co-culture and very low in singly cultured HT29-MTX cells, being detectable in some replicate cultures.

Imaging in negative ionisation mode showed that when the seeding density of Caco2 cells was decreased, the abundance of eicosadienoic acid (20:2) and eicosanoic acid (20:1) tended to decrease, suggesting that these lipids originated from Caco2 cell cultures (Fig. 4). Lyso-phosphatidic acid (18:4) was found to be more abundant in the 25 : 75 co-culture and HT29-MTX culture, while PE (32:1) was unevenly distributed, tending to be more abundant in the co-cultures compared to either Caco2 or HT29-MTX cells cultured alone.

Further data analysis was performed to be able to distinguish where Caco2 and HT29-MTX cells were localised in the co-culture samples. A workflow was developed, which consisted of building and validating a PCA and linear discriminant analysis (LDA) statistical model, using the prototype AMX Imaging software with DESI imaging datasets for the singly cultured Cacao2 and HT29-MTX cells (ESI Fig. S10†). When the model was applied to the DESI imaging datasets collected in both positive and negative ionisation modes for Caco2 : HT29-MTX cell cultures seeded at ratios of 75 : 25, 50 : 50, and 25 : 75, it allowed the different cell types to be identified in the DESI images (Fig. 5). The ratio of pixels is correlated with the ratio of the cell lines used for seeding of the co-culture and showed the heterogeneous way in which the co-cultures grow. Thus, although the 25 : 75 seeding ratio of HT29-MTX : Caco2 cells resulted in a distribution of the HT29-MTX cells within the Caco2 cells, this distribution was not achieved when seeding at a ratio of 75 : 25. This might reflect the difficulty of resuspending the Caco2 cells in the HT29-MTX cells because of the mucus that they produce.

Discussion

DESI-MS imaging has been applied for the first time to the analysis of two important cell models of the gut epithelium, which has allowed the spatial distribution of the distinct lipid species to be mapped. CE (16:2), PCs (16:0_16:1) and TG (48:9) were reproducibly detected in both cell lines and their greater abundance in Caco2 cells, along with the exclusive presence of

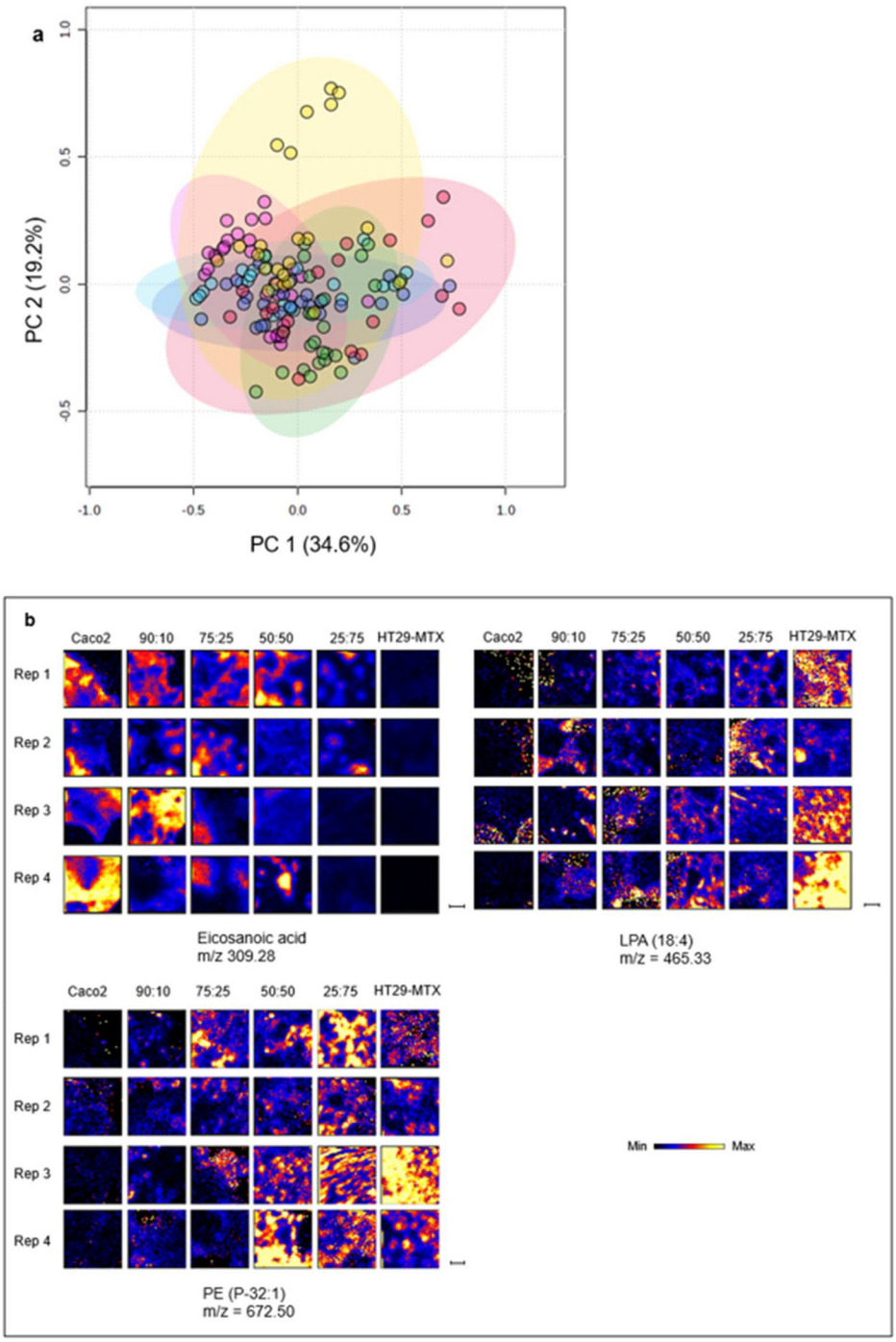

Fig. 4 Comparison of the spatial distribution of lipids in co-cultures of Caco2 and HT29-MTX cells imaged in negative ionisation mode. (a) PCA of ROIs, 0.05 mm^2 for each MS image, each dot representing one ROI coloured as follows: red – Caco2 cells; yellow – HT29-MTX; green – co-culture seeded with a ratio of Caco2–HT29-MTX cells of 90 : 10; purple – co-culture seeded with a ratio of Caco2–HT29-MTX cells of 75 : 25; blue – co-culture seeded with a ratio of Caco2–HT-29MTX cells of 50 : 50; pink – co-culture seeded with a ratio of Caco2–HT-29MTX cells of 25 : 75. Loadings (Fig. S10†) were used to identify lipids responsible for the clustering of ROIs; the distribution of these was then visualised across images (b). The scale bar = 0.05 mm. Lipid identifications are summarised in Table 1.

CE (14:1) in Caco2, is consistent with their known capacity to synthesise cholesterol and cholesterol esters, phosphatidylcholines and triglycerides.[6,30] The greater abundance of these lipids in Caco2 cells may reflect their being more enterocyte-like and hence having the capacity to absorb and re-synthesise lipids. HT29-MTX cells have been less well characterised with regard to their lipid composition and, as a goblet cell model, are less active with regard to lipid uptake and re-synthesis of

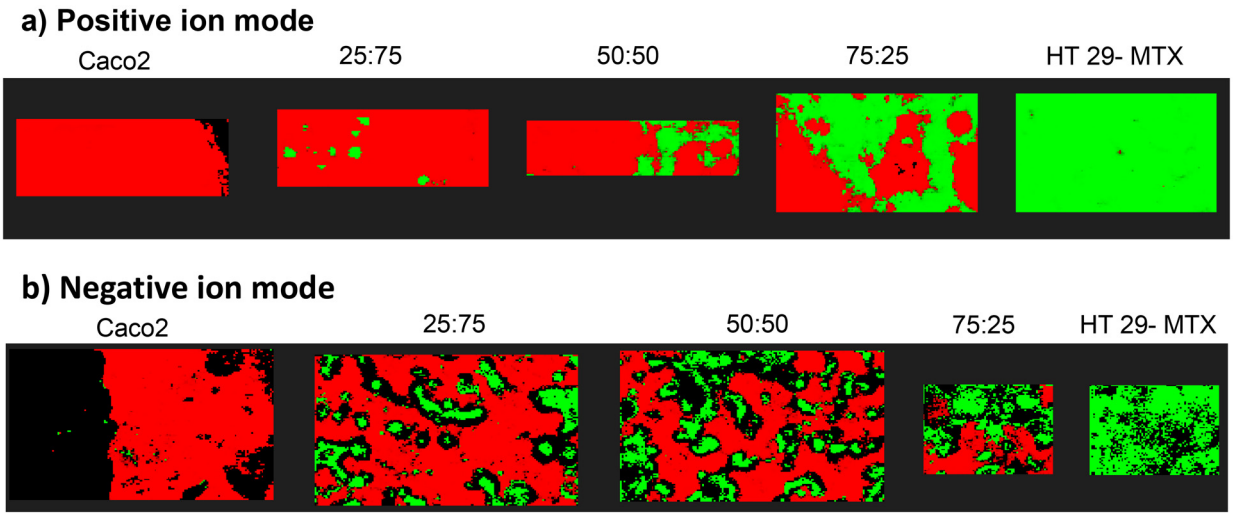

Fig. 5 Mass spectrometry imaging of Caco2 and HT-29-MTX cells within co-cultures in positive (a) and negative (b) ionisation modes. Pixel classification images resulted from the application of a statistical model built based on DESI imaging datasets of either 100% Caco2 or 100% HT29-MTX cells. Pixels classified as Caco2 cells are coloured green, while pixels classified as HT29-MTX cells are coloured red and black pixels were identified either as media or outliers.

triglycerides. In addition to the widespread occurrence of different PC lipid species in cell membranes, it has been found that PCs accumulate on the gut epithelial surface, where they associate with the mucus layer forming a hydrophobic barrier against any bacterial attack.[31,32] This is consistent with the observation in this study of the greater abundance of PCs, including PC (31:1), (16:0_16:1), (16:1_18:1), (O-34:1) and (17:1_18:1) in the mucus-secreting HT29-MTX cells compared to the Caco2 cells. Other types of lipid species, some PEs, LPA (20:0) and PI (36:1) could also be considered as biomarkers for HT29-MTX cell cultures as they were absent in Caco2 cells.

In this study, some lipid species comprised odd chain fatty acid chains, such as PC (31:1) and PC (17:1_18:1). This is an unusual phenomenon since most of the fatty acid chains observed are composed of an even number of carbon atoms since almost all of the total plasma lipids in humans have chain lengths of 2–26 carbon atoms,[33] reflecting the way in which the alkyl chains of lipids are synthesised using building blocks of two-carbon units in the form of acetyl-CoA. Odd-chain fatty acids, such as C15:0, have been identified and are associated with the dietary intake of animal fat in rats, while C17:0 fatty acids appear to be produced as a consequence of endogenous metabolism through α-oxidation.[34] The odd chain fatty acids such as pentadecanoic acid (15:0) and heptadecanoic acid (17:0), have been used as markers of dairy fat intake as they arise from the use of propionate/butyrate in fatty acid synthesis in dairy cattle and are used as biomarkers for dietary food intake evaluation.[35,36] Recent studies reported that the odd-chain fatty acids in human tissue are important biomarkers for the risk of coronary heart disease and type II diabetes mellitus.[37,38] In general, these odd fatty chains are present in trace amounts in most animal tissues,[39] and in this study, most of the lipids that presented an odd carbon number were PCs and were highly distributed in the HT29-MTX cells. Odd-chain fatty acids can be generated through elongation of short chain fatty acids, and this seems an unlikely origin in cells cultured without a microbial source of short-chain fatty acids.[40] One possible origin of the C17 fatty acid is the metabolism of dairy lipids arising from the use of bovine serum in the cell culture medium. Another source might be the shortening of very long chain fatty acid (VLCFAs) through β-oxidation of odd-chain VLCFAs resulting from 2-hydroxylated fatty acids as a consequence of peroxisomal α-oxidation.[40] It therefore seems likely that the odd-chain fatty acids are produced through an endogenous synthetic pathway, which is only present in the HT29-MTX cells.

The MS imaging also showed differential distribution of lipids across the cell cultures, with some lipids clustered in certain regions of the 2D culture, with both cell lines showing heterogeneity across the replicate cultures, especially for the Caco2 cells. This may reflect the way in which Caco2 cells terminally differentiate upon reaching confluence. There is evidence from transcriptome analysis that the co-culture system influences the repertoire of proteins expressed in Caco2 cells, with lipids playing an important role in mediating these changes.[11] Although this study indicates that the lipid profile of HT29-MTX cells was clearly distinguishable, even in the co-culture system, further analysis would be required to ascertain whether the Caco2 cell lipid metabolism is also altered in the presence of HT29-MTX cells, using alternative imaging methodologies, in particular with sub-cellular resolution, which would also help identify the sub-cellular compartment from which the odd chain fatty acids originate. Application of quantitative MS imaging methods would also provide confirmation of the observations made here.[41]

Conclusions

DESI-MS imaging is a rapid, sensitive and accurate technique that can be applied to the investigation of lipid heterogeneity in the 2D cultures of Caco2 and HT29-MTX cells with minimal sample treatment. It has provided insight into the inherent heterogeneity of the cell cultures and has the potential to act as a quality control tool for monitoring and assessing how well they replicate the metabolism and cellular heterogeneity of *ex vivo* gut epithelial tissue and organoids. It is becoming evident that dietary lipids, such as oleic acid[12] and short chain fatty acids originating from either metabolism of dietary compounds or from the microbiota, may be transformed by these different cell types.[5,34] Understanding how such compounds might modify the lipidome of these intestinal cell models will be important as they are increasingly used in an elaborated form to investigate the impact of gut uptake on other cell types ranging from adipocytes to studying inflammation.[42,43] The application of high-resolution DESI-MS imaging provides complementary information to conventional LC-MS/MS lipidomics by adding spatial context to the lipid distributions. It paves the way to targeted DESI-MS imaging of specific lipids of interest that are up- or down-regulated in response to different conditions or treatments. When combined with the PCA-LDA classification tool, this approach enables the interpretation of spatial localisation data, helping to identify a metabolic fingerprint that is unique to either enterocyte-like Caco2 cells or mucus-secreting HT29-MTX cells under co-culture conditions. Additionally, this approach could support the identification of representative local lipid biomarkers or therapeutic targets in more complex systems such as tissue biopsies.

Future application of chemical imaging technology, such as DESI-MS used in this study, will allow spatial metabolomics to be undertaken at both the tissue and the single-cell level, increasing our understanding of how well these cell culture systems model the gut epithelium and identify ways in which they can be improved to better replicate the heterogeneity found *in vivo*.[44]

Author contributions

The work was initiated and conceived by CM and LG; HM and QX undertook the cell culture work, MS imaging data collection and data analysis. EC supervised and undertook the MS imaging analysis. QX, HM, EC and CM drafted the manuscript, and LG reviewed the manuscript.

Conflicts of interest

EC and LG are employees of Waters Corporation, the vendor of mass spectrometry equipment used in this study. QX is currently employed by the University of Surrey on a Knowledge Transfer Partnership project with Waters Corporation but undertook the current work as a PhD student at the University of Manchester. All other authors have no interests to declare in relation to the submitted work.

Data availability

The metabolomics data have been deposited to MetaboLights[45] repository with the study identifier MTBLS12599.

Acknowledgements

We would like to thank Chiara Nitride, Charlotte Hands and Matthew Daly for helpful discussions and support. HM completed this work as a PhD student funded by Al-Baha University in Saudi Arabia.

References

1 I. D. Angelis and L. Turco, *Curr. Protoc. Toxicol.*, 2011, **47**, 20.6.1–20.6.15.
2 R. P. Glahn, G. M. Wortley, P. K. South and D. D. Miller, *J. Agric. Food Chem.*, 2002, **50**, 390–395.
3 V. N. Tran, J. Viktorová and T. Ruml, *Toxins*, 2020, **12**, 628.
4 J. Wen and J. F. Rawls, *Cell Host Microbe*, 2020, **27**, 314–316.
5 R. Shamir, W. J. Johnson, R. Zolfaghari, H. S. Lee and E. A. Fisher, *Biochemistry*, 1995, **34**, 6351–6358.
6 M. Mehran, E. Levy, M. Bendayan and E. Seidman, *In Vitro Cell. Dev. Biol.: Anim.*, 1997, **33**, 118–128.
7 A.-C. Schneider, E. Mignolet, Y.-J. Schneider and Y. Larondelle, *Br. J. Nutr.*, 2013, **109**, 57–64.
8 F. Yang, G. Chen, M. Ma, N. Qiu, L. Zhu and J. Li, *Lipids Health Dis.*, 2018, **17**, 1–14.
9 M. W. Werno, I. Wilhelmi, B. Kuropka, F. Ebert, C. Freund and A. Schürmann, *Biochem. Biophys. Res. Commun.*, 2018, **506**, 259–265.
10 V. Hiebl, D. Schachner, A. Ladurner, E. H. Heiss, H. Stangl and V. M. Dirsch, *Biol. Proced. Online*, 2020, **22**, 1–18.
11 E. Berger, M. Nassra, C. Atgié, P. Plaisancié and A. Géloën, *Int. J. Mol. Sci.*, 2017, **18**, 1573.
12 A. Wikman-Larhed and P. Artursson, *Eur. J. Pharm. Sci.*, 1995, **3**, 171–183.
13 I. Lozoya-Agullo, F. Araujo, I. Gonzalez-Alvarez, M. Merino-Sanjuan, M. Gonzalez-Alvarez, M. Bermejo and B. Sarmento, *Mol. Pharm.*, 2017, **14**, 1264–1270.
14 P. Hoffmann, M. Burmester, M. Langeheine, R. Brehm, M. T. Empl, B. Seeger and G. Breves, *PLoS One*, 2021, **16**, e0257824.
15 J. Elzinga, M. Grouls, G. Hooiveld, M. van der Zande, H. Smidt and H. Bouwmeester, *Arch. Toxicol.*, 2023, **97**, 737–753.
16 A. C. Pelosi, A. A. R. Silva, A. M. A. P. Fernandes, P. P. M. Scariot, M. S. P. Oliveira, A. M. Porcari, D. G. Priolli and L. H. D. Messias, *Front. Biomed.*, 2024, **11**, 1436866.

17 G. Tolle, G. Serreli, M. Deiana, L. Moi, P. Zavattari, A. Pantaleo, C. Manis, M. A. El Faqir and P. Caboni, *Int. J. Mol. Sci.*, 2024, **25**, 12638.
18 K. El Hindi, S. Brachtendorf, J. C. Hartel, C. Renné, K. Birod, K. Schilling, S. Labocha, D. Thomas, N. Ferreirós and L. Hahnefeld, *Biochim. Biophys. Acta, Mol. Basis Dis.*, 2024, **1870**, 166906.
19 A. P. Bowman, R. M. Heeren and S. R. Ellis, *TrAC, Trends Anal. Chem.*, 2019, **120**, 115197.
20 E. A. Bonnin and S. O. Rizzoli, *Front. Behav. Neurosci.*, 2020, **14**, 124.
21 A. R. Buchberger, K. DeLaney, J. Johnson and L. Li, *Anal. Chem.*, 2017, **90**, 240.
22 K. A. Zemski Berry, J. A. Hankin, R. M. Barkley, J. M. Spraggins, R. M. Caprioli and R. C. Murphy, *Chem. Rev.*, 2011, **111**, 6491–6512.
23 L. S. Eberlin, C. R. Ferreira, A. L. Dill, D. R. Ifa and R. G. Cooks, *Biochim. Biophys. Acta, Mol. Cell Biol. Lipids*, 2011, **1811**, 946–960.
24 N. E. Manicke, J. M. Wiseman, D. R. Ifa and R. G. Cooks, *J. Am. Soc. Mass Spectrom.*, 2008, **19**, 531–543.
25 J. D. Ewald, G. Zhou, Y. Lu, J. Kolic, C. Ellis, J. D. Johnson, P. E. Macdonald and J. Xia, *Nat. Protoc.*, 2024, 1–31.
26 J. Balog, T. Szaniszlo, K. C. Schaefer, J. Denes, A. Lopata, L. Godorhazy, D. Szalay, L. Balogh, L. Sasi-Szabo, M. Toth and Z. Takats, *Anal. Chem.*, 2010, **82**, 7343–7350.
27 M. De Graeve, N. Birse, Y. Hong, C. T. Elliott, L. Y. Hemeryck and L. Vanhaecke, *Food Chem.*, 2023, **404**, 134632.
28 J. Balog, D. Perenyi, C. Guallar-Hoyas, A. Egri, S. D. Pringle, S. Stead, O. P. Chevallier, C. T. Elliott and Z. Takats, *J. Agric. Food Chem.*, 2016, **64**, 4793–4800.
29 A. P. Walczak, E. Kramer, P. J. Hendriksen, P. Tromp, J. P. Helsper, M. Van Der Zande, I. M. Rietjens and H. Bouwmeester, *Nanotoxicology*, 2015, **9**, 453–461.
30 S. R. Cerda, J. Wilkinson IV and S. A. Broitman, *Lipids*, 1995, **30**, 1083–1092.
31 A. Korytowski, W. Abuillan, F. Amadei, A. Makky, A. Gumiero, I. Sinning, A. Gauss, W. Stremmel and M. Tanaka, *Biochim. Biophys. Acta, Biomembr.*, 2017, **1859**, 959–965.
32 R. Ehehalt, J. Wagenblast, G. Erben, W. D. Lehmann, U. Hinz, U. Merle and W. Stremmel, *Scand. J. Gastroenterol.*, 2004, **39**, 737–742.
33 K.-T. Khaw, M. D. Friesen, E. Riboli, R. Luben and N. Wareham, *PLoS Med.*, 2012, **9**, e1001255.
34 B. J. Jenkins, K. Seyssel, S. Chiu, P.-H. Pan, S.-Y. Lin, E. Stanley, Z. Ament, J. A. West, K. Summerhill and J. L. Griffin, *Sci. Rep.*, 2017, **7**, 1–8.
35 T. M. Venäläinen, M. A. Lankinen and U. S. Schwab, *Am. J. Clin. Nutr.*, 2017, **106**, 954.
36 K. Dornan, A. Gunenc, B. D. Oomah and F. Hosseinian, *J. Am. Oil Chem. Soc.*, 2021, **98**, 813–824.
37 K. Kurotani, P. Karunapema, K. Jayaratne, M. Sato, T. Hayashi, H. Kajio, S. Fukuda, H. Hara, O. Okazaki and A. U. Jayatilleke, *Nutr. Res.*, 2018, **50**, 82–93.
38 N. R. Matthan, E. M. Ooi, L. Van Horn, M. L. Neuhouser, R. Woodman and A. H. Lichtenstein, *J. Am. Heart Assoc.*, 2014, **3**, e000764.
39 A. E. Smedman, I.-B. Gustafsson, L. G. Berglund and B. O. Vessby, *Am. J. Clin. Nutr.*, 1999, **69**, 22–29.
40 M. Pfeuffer and A. Jaudszus, *Adv. Nutr.*, 2016, **7**, 730–734.
41 M. Vandenbosch, S. M. Mutuku, M. J. Q. Mantas, N. H. Patterson, T. Hallmark, M. Claesen, R. M. A. Heeren, N. G. Hatcher, N. Verbeeck, K. Ekroos and S. R. Ellis, *Anal. Chem.*, 2023, **95**, 18719–18730.
42 E. Berger and A. Géloën, *Adipocyte*, 2019, **8**, 83–97.
43 M. del C. Ponce de León-Rodríguez, J.-P. Guyot and C. Laurent-Babot, *Crit. Rev. Food Sci. Nutr.*, 2019, **59**, 3648–3666.
44 M. J. Taylor, J. K. Lukowski and C. R. Anderton, *J. Am. Soc. Mass Spectrom.*, 2021, **32**, 872–894.
45 O. Yurekten, T. Payne, N. Tejera, F. X. Amaladoss, C. Martin, M Williams and C. O'Donovan, *Nucleic Acids Res.*, 2024, **52**(D1), D640–D646.